Doping content dependencies on the structure modification and bandgap broadening of Al induced sol-gel derived ZnO nanostructures

Marina Marzuki*, Mohd Zamzuri Mohammad Zain, Wan Abd Rahman Assyahid Wan Ibrahim, Nooraizedfiza Zainon and Rozie Nani Ahmad

Faculty of Mechanical Engineering Technology, Universiti Malaysia Perlis (UniMAP), Perlis, MALAYSIA

ABSTRACT

This paper reports the Al doping content dependence on structure modification and band gap widening of sol-gel synthesised Al-doped ZnO thin films. The precursor, solvent and stabiliser used to prepare ZnO solution were Zinc Acetate Dihydrate, 2-propanol and ethanolamine, respectively. Molarity fractions of 0, 4, 6 and 8% of Al $(NO_3)_2$ as dopant source was incorporated into ZnO host system and prepared by individual buffer solutions. The prepared sols were subsequently deposited onto ITO glass substrates, and the resultant thin films were characterised. XRD patterns exhibit the polycrystalline nature of pure and doped ZnO films, with preferred orientations correspond to (1 0 0), (0 0 2) and (1 0 1) planes. Lattice shrinking is indicated by the decrease lattice constant c due to axial compression. Peaks shifting towards higher angle are observed implying a structural modification over doped thin films that affects the optical properties, which agrees with the lattice shrinking. The absorption edge has an obvious blueshift to the shorter wavelength with increased dopant content. The thin films' energy bands were procured by Tauc's linear extrapolation and was found to be broadening from 3.32 eV to 3.34 eV in 6% Al-doped ZnO. There exists a significant correlation between the applied doping level and the extend of variation of structural properties and ultimately, lattice imperfection. Doping of smaller-atom-sized Al into ZnO concedes with the Burstein-Moss principles. 6% Al doping imposes the highest peak shift and ultimately has the highest impact on lattice parameter and energy band.

Keywords: Al-doped ZnO, sol-gel, blueshift, bandgap, lattice shrinking

1   INTRODUCTION

With its high exciton binding energy (60 meV) and broad direct bandgap, zinc oxide (ZnO) have been the focus point of extensive researches in sensors, thin-film solar cells and thin-film applications. The developed ZnO films typically possesses n-type conductivity due to interstitial zinc and gas vacancies or/and intrinsic defects [1]. The properties of ZnO can be enhanced by extrinsically doping a small amount of impurity. For instance, to expand ZnO host system's bandgap, wider bandgap elements are incorporated into the host's lattice. Dopant intrinsically creates a Fermi lift that would effectively widen the energy gap between the conduction band (CB) and the valence band (VB) [2]. Wide bandgap semiconductor tends to absorb high energy wavelength due to blue

---

shift in absorption edge, thus becoming a contributing factor in enhancing solar conversion efficiency. Several researches have reported that the reduction of a semiconduc crystal size is associated with bandgap broadening [3]–[6]. Because of this, higher absorbance of quantum energy supplied by photons with higher eV is anticipated for VB-to-CB excitations, and consequently shifting of absorption edge. Blueshift effect is mostly encountered when there is a crystal size reduction near to the exciton radius in bulk semiconductor (between 2-30 nm); and such particles are identified as "quantum dots". With the presence of dopant in the host crystal lattice, lattice defects together with deviation from perfect crystallinity are characterised by structural parameters including lattice distortion, microstrain, crystallite size and crystal orientations. In a bottom-up perspective, these attributes are the main driving force for structure-dependent semiconductors such as ZnO.

There is a wide range of growth and properties on ZnO and Al-doped ZnO nanostructures employing different synthesis methods. Among others are sputtering, electrodeposition (EDP) molecular beam epitaxy (MBE) and chemical vapor deposition (CVD). Additionaly, sol-gel spin coating technique offers simple experimentation setups, shorter lead times, high yield and economical. In this study, pure and Al-doped ZnO thin films with different Al content by sol-gel spin coating method are used.

Since the establishment of Group III impurities as dopant, Al incorporation into ZnO has been acknowledged as a free carrier's donor and at the same time, maintaining good transparency in the visible light wavelength spectrum [7]. The incorporation of Al in ZnO parent system has been proved feasible in realising the properties improvement. Addition of Al into ZnO was reported by Xu et al. [8], in which as the Al concentration increase, the near band edge (NBE) emission peak has a blueshift towards a higher photon energy region. Bandgap broadening with an obvious blueshift of absorption edge was reported by Zhai et. al. [9]. According to these, the Burstein -Moss (BM) effect was indicted for interpreting the widening in many literatures. While it is generally accepted that the BM effect would cause bandgap broadening of ZnO, the detailed structural aspect responsible for the bandgap broadening poorly understood and remain a subject of contradictory views. Islam et al. [10] documented that Al dopant substitution in ZnO leads to bandgap narrowing. The decrease in E_g value with increasing Al incorporation clashed with the material's shrinking crystal size. This is somewhat contradictory with the growth of bandgap relations to small crystallites. Likewise, Mahdavi et. al. [11] claimed that the bandgap narrowing phenomenon by increasing Al content is due to Al^{3+} role as a sideway band that creates an excessive energy surface between the conduction and valence band, thus reducing the bandgap. Due to this, this paper intends to provide a fresh view on the correlation between the extent of variation of structural properties implied by Al doping to optical properties, especially on the bandgap widening of ZnO thin films.

2   EXPERIMENTAL PROCEDURE

0.1M of Zn^{2+} sol-gel was prepared by dissolving zinc acetate dehydrate ($CH_3(COOH)_2$) precursor in 2-propanol by vigorous stirring at 600 rpm and temperature 50°C for 60 minutes. Subsequently, an equimolar concentration of ethanolamine stabilizer was added dropwise. At this stage, a homogenous and clear solution is obtained. The stirring was continued for 30 minutes; and the prepared solution was allowed to cool down to room temperature for 24 hours. The preparation of Al doped ZnO sol-gel followed the same procedure as pure ZnO solution with addition of $Al(NO)_3$ as dopant source with molarity fractions of 4% , 6% and 8%. Meanwhile, ITO coated glass substrates were pretreated in acetone, followed by NaOH bath and rinsed with deionised water prior to deposition. Thin films are synthesised by depositing the solutions onto the substrates via

spin coating at rotational speed of 3000 rpm for 30 s. The deposition is repeated three times to obtain a smooth and uniform film and finally annealed for 60 minutes at 400°C in crucible furnace.

The structural examination was performed with X ray diffraction (XRD) analysis with CuKα radiation, α =1.5406 Å, 0.2°/s scan step and diffraction angle between 20° to 80°. The surface topologies of the deposited ZnO thin films were visualized with Atomic Force Microscopy (AFM).The material's elemental composition was observed by Energy Disperse Spectroscopy (EDS) analysis. The transmittance spectra of the thin films was observed with Ultra violet Visible Spectroscopy (Uv-Vis) at wavelength range between 200 to 900 nm.

3   RESULT AND DISCUSSION

3.1   Structural analysis

The crystallographic study and preferred orientations of the thin films influenced by Al incorporation in ZnO host composite system have been performed with XRD. The peak analysis shows that the films have preferred orientations corresponding to (100), (002) and (101) planes (Fig. 1). These planes correspond to hexagonal wurzite structure and comply with the crystal identities in ICDD card No. 00-005-0664. The diffraction peaks broadening is observed by increase of FWHM (Table 1) with an increase in Al doping content, which potrays the degradation of crystallinity and crystal size reduction of the prepared thin films. This also reflects that the Al substitution in the ZnO matrix promotes defects in the lattice site [12]. The presence of multiple peaks without a dominant one also indicates a polycrystalline nature of the synthesised thin films. Concurrently, an obvious shifting towards higher diffraction angle was observed on the doped films. The shifting implies that Al is being successfully incorporated into ZnO lattice [13]. Furthest shifting is observed on the 6% Al-doped ZnO thin film.
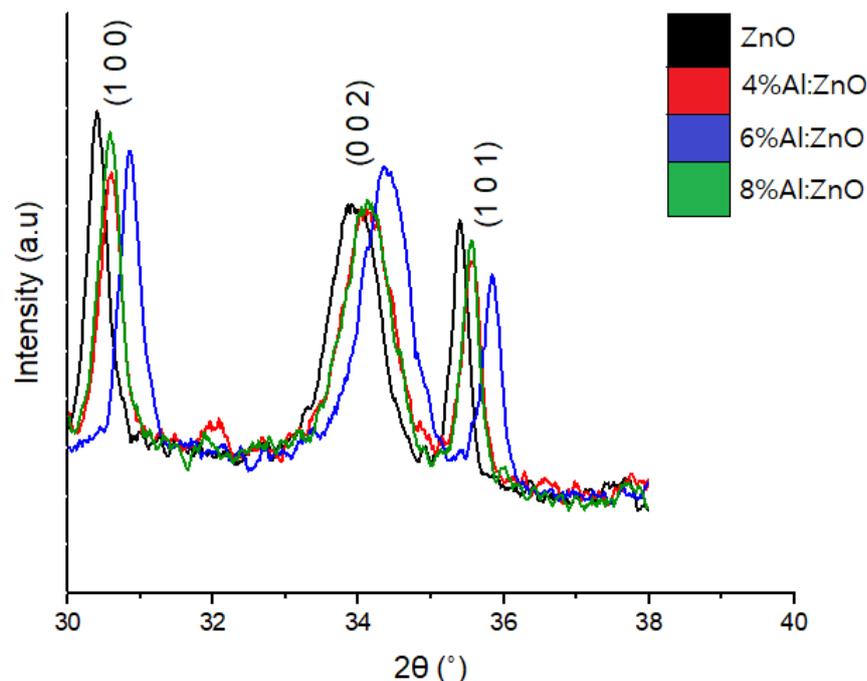

Fig. 1: XRD pattern (zoom) of the preferred peaks showing a clear shiting towards higher angle

Table 1: Structural parameter of ZnO and Al doped ZnO thin films

Sample	hkl	Peak position, $2\theta(°)$	Lattice spacing, d (Å)	FWHM, β (rad)	Crystal size, D (nm)
ZnO	100	30.4173	2.936	0.3193	45
	002	34.0576	2.63	0.6989	20
	101	35.3722	2.5352	0.35374	41
4%Al:ZnO	100	30.5791	2.9208	0.3266	44
	002	34.179	2.6209	0.7184	20
	101	35.5744	2.5213	0.42433	34
6%Al:ZnO	100	30.8622	2.8946	0.3266	44
	002	34.4216	2.603	0.7184	20
	101	35.8576	2.5020	0.36126	40
8%Al:ZnO	100	30.5993	2.9189	0.3413	42
	002	34.1992	2.6194	0.6863	21
	101	35.5946	2.5199	0.4544	32

Furthermore, other structural parameters were evaluated by referring to the peak profiles (Table 1). Interplanar spacing, *d* was obtained by the following formula:

$$d = \frac{n\lambda}{2\sin\theta} \qquad (1)$$

The order of diffraction is noted by n=0.9 , λ is the incident CuKα X- ray wavelength (1.5406 Å) and θ is referred to the deflection angle of the respective plane. The shifting of the peaks resulted in a decrease of interplanar spacing, *d* (Table 1). Crystallite size (*D*) was calculated by referring to the Scherrer approach:

$$D = \frac{0.9\lambda}{\beta\cos\theta} \qquad (2)$$

where β is the FWHM of the respective peak in radian. A reduction is observed in *D*. Diversely, crystal quality deterioration can be summarised from the FWHM increase, indicated by the peak broadening parallel with doping content. This condition is due to the reduction of Zn interstitials for charge compensation, results in suppressed ZnO growth and reduced crystallinity [14]. Lattice constants, *a* and *c* are attained from the (1 0 0) and (0 0 2) peak positions with the following equations [15]:

$$a = \frac{2}{\sqrt{3}} d_{100} \qquad (3)$$

$$c = 2d_{002} \qquad (4)$$

where *d* is the interplanar spacing of the peaks. These constants decrease with the increase of the dopant's concentration (Fig. 2). The XRD peak shifting to higher value of θ can be directly linked to the shrinkage of the lattice parameters . This condition can be associated with Zn^{2+} (ionic radius 0.60 Å) substitution by smaller Al^{3+} (ionic radius 0.58 Å) into ZnO that yields in lattice shrinkage The dopant induced lattice shrinking- higher angle peak shift relation also agrees with the Bragg's principle [16]. The value of *c* of doped thin films is smaller than pristine ZnO film which explains that an axial compression acts on the *c*-axis [17].
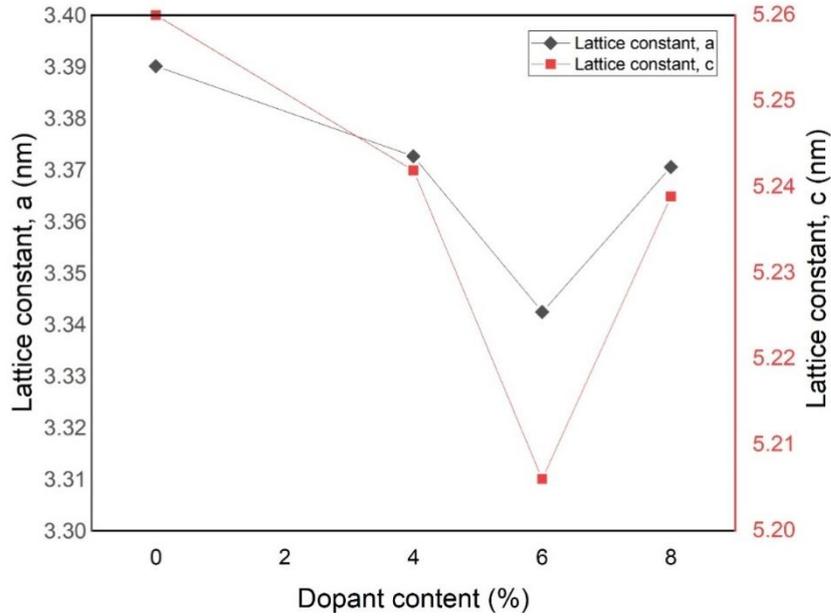
Fig. 2: Lattice constants (a and c)

Subsequently, the dislocation density, δ which can be interpreted to the extent of defects in the films was estimated by referring to Williamson and Smallman's formula [18]:

$$\delta = \frac{1}{D^2} \qquad (5)$$

Micro-strain, ε have been estimated by referring to the following Williamson-Hall relations [19]:

$$\varepsilon = \frac{\lambda}{D \cos \theta} - \frac{\beta}{\tan \theta} \qquad (6)$$

The estimated values are tabulated in Table 2. Microstrain in this context is defined as a slight slip in lattice position as regards to regular lattice position. It is observed that the dislocation density and microstrain increased along with doping content. As per calculated result, the dislocation density and microstrain can be directly linked to the crystallite size reduction and the shifting of the diffraction peaks. The effect is mainly resulting from the synthesis condition and mechanical effects [20]. The effect is most pronounced on the (100) orientation. Furthermore, regarding the static parameter and its variations, stacking fault measurement within the crystal structure provides an additional information of the host nanostructure and its spatial arrangements. The stacking fault probability, γ is the stacking sequence fault sustained by a fraction of layers in a given crystallite structure hence, at least a faulty is anticipated to be found in $1/\gamma$ layer. This circumstance can be attributed by the shifting of the diffraction peak position. The stacking fault probability, γ with respect to the shifting of the respective peak, $\Delta(2\theta)$ is estimated by [21]:

$$\gamma = \frac{2\pi^2}{45\sqrt{3}} \frac{\Delta(2\theta)}{\tan \theta_{hkl}} \qquad (7)$$

where $\Delta(2\theta)$ is the shift in peak position and θ_{hkl} is the diffraction angle corresponding to the preferred orientation. The alterations of the lattice parameters with regards to doping content are due to the mechanics contributed by the secondary phase onto host lattice such as distortion, expansion, dislocation and coherency stress [22]. It is also observed that Al doping induces low stacking fault probability, thus the stoichiometry between Al doping content and structural parameters change in this study can be referred.

Table 2: Mechanical parameter of pristine and doped ZnO

Sample	hkl	Lattice distortion, δ	Microstrain, ε	Stacking fault probability, γ
ZnO	100	0.0004939	1.1709	0 (ref)
	002	0.0023227	2.2738	0 (ref)
	101	-		0 (ref)
4%Al:ZnO	100	0.0005163	1.1909	0.0016
	002	0.0024522	2.3282	0.0001
	101	-		0.0005
6%Al:ZnO	100	0.0005156	1.1795	0.0069
	002	0.002449	2.3107	0.0001
	101	-		0.0016
8%Al:ZnO	100	0.0005637	1.2437	0.0019
	002	0.0022379	2.2228	0.0001
	101	-		0.0006

Al in ZnO host can act as amphoteric dopant, in which can either exists in substitutional Zn sites or in the interstitial sites; or both [23]. While lattice shrinkage can be straightforwardly associated with smaller-Al substitution theory as can be observed with 0 to 6 % doping content (Fig. 2), the extra doping content at 8% shifts the peaks back to lower angle. This may be contributed by the undoped Al interstitially positioned itself between the Zn lattices, hence the peak shift slightly to lower angle. For a particular point defect such as interstitials, the local stress in their vicinity could disturb the order of the host's lattice plane given an adequate concentration [24]. The interstitial position of of smaller Al relieves the local compressive stress in Zn lattice which can be observed by the reduction of lattice distortion and microstrain of 8% doped sample as compared to 6% doped sample (Table 2).

3.2   Surface morphology analysis

The surface topography of the pure and Al-doped ZnO thin films is obtained by AFM observations. In the pure ZnO film, large, dense and irregular grains are seen which are distributed throughout the surface (Fig. 3). Such surface morphology can be anticipated for ZnO film deposited by spin coating method [25]. It is may be associated with the use of seed layer to efficiently prepare a well-grown thin film for site selective nucleation [26]. In this study, the compact nuclei are achieved due to the seed layer ITO; thus the crystal quantity formed in the early stage of growth can also be high. With the integration of Al doping, the spherical grain features changed to smaller pointy aggregates. These are formed by aggregation of nanoscaled crystallites. Dopant substitution, with its smaller radius than the host's causes lattice shrinkage during nucleation stage and produces smaller grains [27]. By referring to Vegards' law [28], this is expected in Al incorporated ZnO composites due to the aforementioned ionic radius difference. This condition agrees with other similar reported findings [26–28]. Furthermore, the correlation between Al doping content to the root min square (RMS) roughness and average grain size of the pure and undoped films were also observed. Although the crystallite size is further reduced linearly with doping concentration, agglomeration started to form (Fig. 3b, c & d). The reduction of individual particle size promotes high surface-to-volume ratio, consequently increase the surface free energy that tends to attract other particles. This condition could also be linked to the sol-gel synthesis process, in which during the nucleation stage, the particles dispersed in liquid phase stick to each other and immediately form irregular particle assemblages or aggregates [32]. The aggregation affected the surface

roughness and intensified as the dopant concentration increase. The aggregation, and accordingly the pores enlarging are most pronounced in 8% doped ZnO (Fig. 3d).
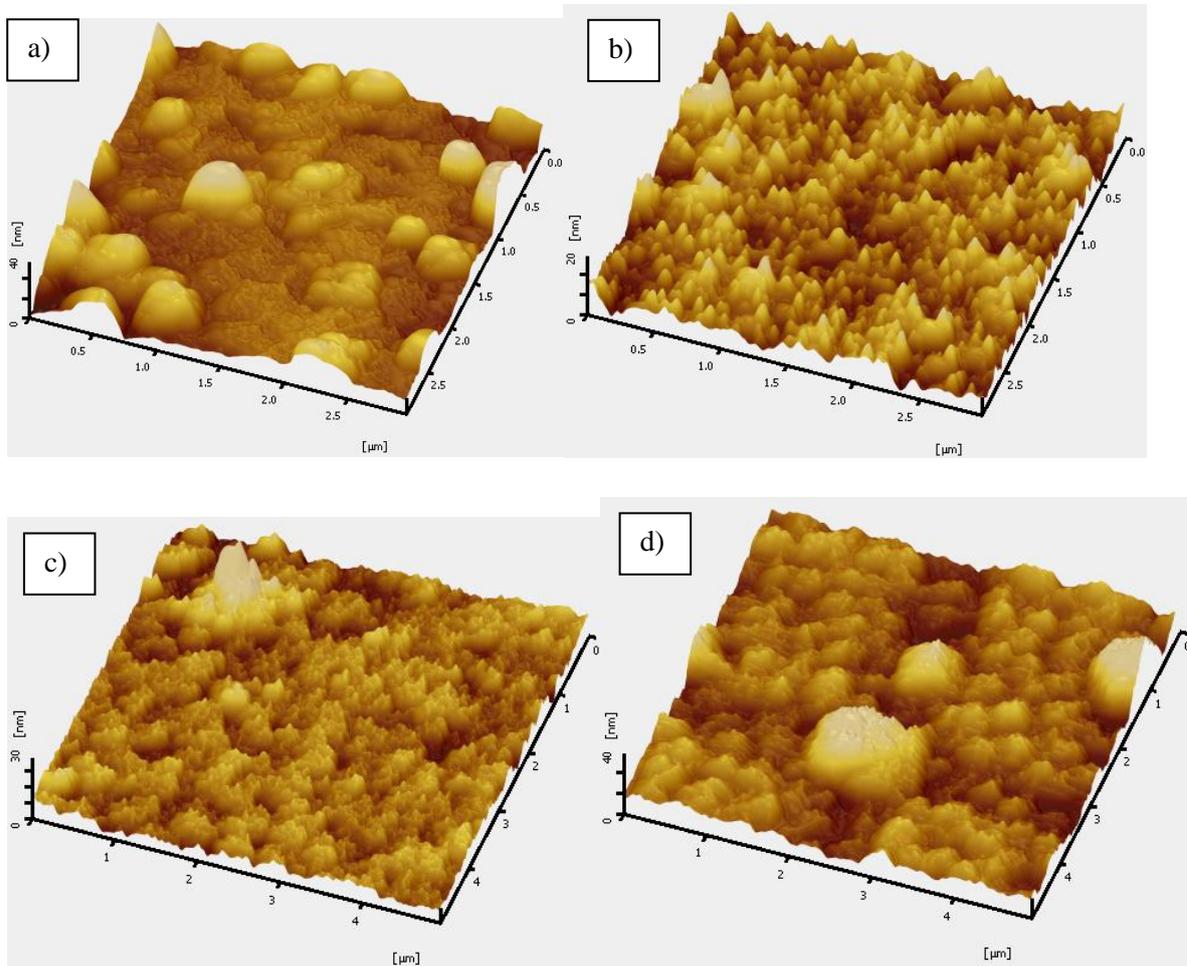

Fig. 3: AFM surface topography of undoped and Al-doped ZnO thin films

3.3 Compositional analysis

Elemental compositions of the thin films were obtained by EDS spectra analysis (Fig. 4). From the analysis' finding, the purity of the pristine and Al-doped ZnO was confirmed. Based on the observation, it is distinctive that the samples contain only Zn, Al and O elements. The Zn content drops with the increase of Al concentration furthers affirmed the Al substitution into ZnO lattice. Aside from that, the lattice mismatch defects caused by this factor promotes sites for oxygen inhibitions, indicated by the rise in oxygen fraction. The rise in oxygen also further proposed the bandgap widening effect of the doped thin films. This is predicted based on the contradictory redshift of absorption edge followed by bandgap narrowing due to oxygen vacancy [30, 31] and bandgap widening due to oxygen-induced oxide thin films [35]. In the 8% Al-doped film, the dominant content of oxygen could possibly be supplied by the amorphous states of Al_2O_3 grown by undoped Al into the ZnO lattice, that are interstitially positioned between the ZnO grains [36]. Wang et. al. [36] also reported that the peaks belong to Al_2O_3 could not be observed in XRD spectra due to its high formation enthalpy.
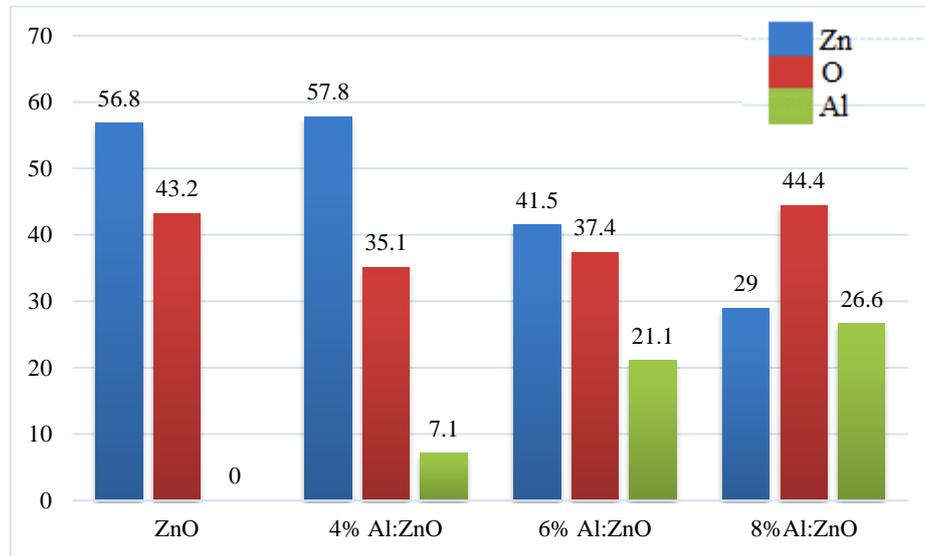
Fig. 4: Elemental compositions of the thin films by EDS analysis

3.4   Optical characteristics

The absorbance spectra has been observedd by uv-vis spectroscopy. Subsequently, the transmittance of the thin films (Fig. 5) is obtained by Beer's equation as follows:

$$\%T = log^{-1}(2 - A) \quad (8)$$

where *A* refers to the light absorbance of the films. The doped films exhibited an improved light transmission over 80% in the visible range together with a sharp principal absorption edge. This is crucial in transparent conductive oxides and solar device functions. However, it is noted that these finding contradicts with the reported reduction of transmittance with increase of Al content [10]. The reduction is explained due to the reduction of crystallite size of ZnO with Al substitution increase the grain boundary density. This condition consequently caused the optical scattering that would reduce the visible light transmittance. Even so, from the structural result in previous section, we found that there are no significant changes in crystallite size, yet in the AFM topography; it can be oserved that there is a variation in surface contour of the deposited thin film. This variation might explain the different transmittance values. The inset in Fig. 5 exhibits clear absorption edge blueshift to the shorter wavelength on the doped films highlighted by the green circle and arrow pointing the direction of the shift. The blue-shifting manner is one of the

indications of the energy band widening, which is elucidated by the Burstein-Moss theory. To justify the blueshift relations to the change in the energy band, Tauc analysis is performed using the following equation:

$$\alpha h v = A(h v - E g)^{m/2} \quad (9)$$

where m =1 (for direct transition; in this case, ZnO has direct bandgap), h is Planck's constant, v is the frequency of the incident photon while A is the electron-hole mobility constant. The bandgap energy is dictated by extrapolating the linear portion of the absorption edge. The energy bands of the samples are tabulated in Table 3. The energy bands of the thin films are found to be increasing linearly with increasing dopant content and reached a maximum value at 6% Al doping content. Generally, the blueshift of the absorption edge can be linked to the carrier densification that blocks the lower state in the conduction band due to Fermi level lift. The lifting of the Fermi level approaching the conduction band leads to energy band broadening. In addition, the shrinking of the crystallite size of the thin films to nanoscales creates a quantum confinement effect, which is also a contributing factor to the energy band broadening [37]. It is suggested that while the crystallite size reduces, the continuous energy bands then would separate into discrete levels leading to an effective bandgap widening [36].
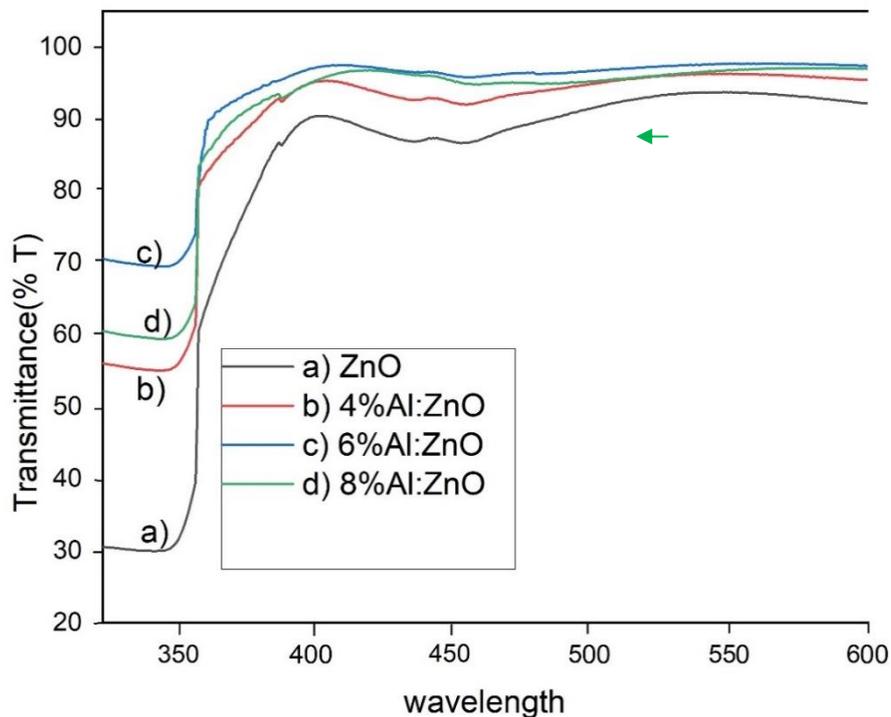
Fig. 5: Transmittance spectra of the undoped and Al doped ZnO thin films. The inset zoom image magnifies the blueshift of absorption edge

Table 3: Energy bands of pure and Al-doped ZnO

Sample	Energy band (hv)
ZnO	3.32
4%Al:ZnO	3.33
6%Al:ZnO	3.34
8%Al:ZnO	3.33

4   CONCLUSION

Pristine and Al-induced ZnO nanocrytalline thin films on ITO glass substrates were synthesised via sol-gel. The effects of Al dopant content on the crystal structure, optical properties, and surface morphology of ZnO films were investigated. The XRD analysis shows that the incorporation of Al dopant has an impact on the structural and optical properties of ZnO thin films. It is observed that a limit of Al content at 6%; which has the highest peak shift and blueshift; therefore signifies there is a structural change that leads to bandgap widening from 3.32 to 3.34 eV which agrees with the Burstein-Moss principle. EDS analysis shows a controlled composition of Zn and O; which is vital in keeping a balanced ratio of Zn and O. On the other hand, in the 8% Al doping concentration thin films, the dominating oxygen content would likely motivates the formation of amorphous Al_2O_3 with the remnants Al which positioned interstitially between ZnO lattices. This resulted in a varied strutural and optical properties of the thin films.

ACKNOWLEDGEMENT

REFERENCES

[1]   J. Kennedy, P. P. Murmu, J. Leveneur, A. Markwitz, and J. Futter, "Ac ce p cr t," *Appl. Surf. Sci.*, 2016, doi: 10.1016/j.apsusc.2016.01.160.

[2]   G. Tang, H. Liu, and W. Zhang, "The variation of optical band gap for ZnO:In films prepared by sol-gel technique," *Adv. Mater. Sci. Eng.*, vol. 2013, pp. 1–5, 2013, doi: 10.1155/2013/348601.

[3]   M. A. Majeed Khan, S. Kumar, M. Naziruddin Khan, M. Ahamed, and A. S. Al Dwayyan, "Microstructure and blueshift in optical band gap of nanocrystalline Al xZn1-xO thin films," *J. Lumin.*, vol. 155, pp. 275–281, 2014, doi: 10.1016/j.jlumin.2014.06.007.

[4]   M. K. Debanath and S. Karmakar, "Study of blueshift of optical band gap in zinc oxide (ZnO) nanoparticles prepared by low-temperature wet chemical method," *Mater. Lett.*, vol. 111, pp. 116–119, 2013, doi: 10.1016/j.matlet.2013.08.069.

[5]   Y. Liu *et al.*, "Effect of Mg doping on the hydrogen-sensing characteristics of ZnO thin films," *Sensors Actuators, B Chem.*, vol. 160, no. 1, pp. 266–270, 2011, doi: 10.1016/j.snb.2011.07.046.

[6]   W. L. Liu and Y. F. Zhang, "Blueshift of absorption edge and photoluminescence in Al doped ZnO thin films," *Integr. Ferroelectr.*, vol. 188, no. 1, pp. 112–120, 2018, doi: 10.1080/10584587.2018.1454222.

[7]   A. Das, G. Das, D. Kabiraj, and D. Basak, "High conductivity along with high visible light transparency in Al implanted sol-gel ZnO thin fi lm with an elevated fi gure of merit value as a transparent conducting layer," *J. Alloys Compd.*, vol. 835, p. 155221, 2020, doi: 10.1016/j.jallcom.2020.155221.

[8]   X. J. XU Zi-qiang, DENG Hong, "Al-doping Effects on Optical Properties of C-axis Orientated ZnO:Al Thin Films Prepared by the Sol-gel Method," *J. Optoelectron.*, vol. 03, 2006.

[9]   C. Zhai *et al.*, "Effects of Al Doping on the Properties of ZnO Thin Films Deposited by Atomic Layer Deposition," *Nanoscale Res. Lett.*, 2016, doi: 10.1186/s11671-016-1625-0.

[10]   M. R. Islam, M. Rahman, S. F. U. Farhad, and J. Podder, "Structural, optical and photocatalysis properties of sol–gel deposited Al-doped ZnO thin films," *Surfaces and Interfaces*, vol. 16, no. February, pp. 120–126, 2019, doi: 10.1016/j.surfin.2019.05.007.

[11]   R. Mahdavi and S. S. A. Talesh, "Sol-gel synthesis , structural and enhanced photocatalytic

performance of Al doped ZnO nanoparticles," *Adv. Powder Technol.*, vol. 28, no. 5, pp. 1418–1425, 2017, doi: 10.1016/j.apt.2017.03.014.

[12]   G. Vijayaprasath, R. Murugan, T. Mahalingam, Y. Hayakawa, and G. Ravi, "Preparation of highly oriented Al:ZnO and Cu/Al:ZnO thin films by sol-gel method and their characterization," *J. Alloys Compd.*, vol. 649, pp. 275–284, 2015, doi: 10.1016/j.jallcom.2015.07.089.

[13]   N. Karak, B. Pal, D. Sarkar, and T. K. Kundu, "Growth of Co-doped ZnO nanoparticles by porous alumina assisted sol-gel route: Structural optical and magnetic properties," *J. Alloys Compd.*, vol. 647, pp. 252–258, 2015, doi: 10.1016/j.jallcom.2015.05.147.

[14]   R. Vettumperumal, S. Kalyanaraman, and R. Thangavel, "A comparative study of structural , surface morphology and optical properties of Na and Mg codoped ZnO nanocrystalline thin films prepared using sol – gel spin coating technique," *J. Mol. Struct.*, vol. 1059, pp. 61–67, 2014, doi: 10.1016/j.molstruc.2013.11.044.

[15]   M. Caglar, Y. Caglar, and S. Ilican, "Investigation of the effect of Mg doping for improvements of optical and electrical properties," *Phys. B Condens. Matter*, vol. 485, pp. 6–13, 2016, doi: 10.1016/j.physb.2015.12.049.

[16]   N. M. Rosas-Laverde, A. Pruna, J. Cembrero, J. Orozco-Messana, and F. J. Manjón, "Performance of graphene oxide-modified electrodeposited ZnO/Cu2O heterojunction solar cells," *Bol. la Soc. Esp. Ceram. y Vidr.*, vol. 58, no. 6, pp. 263–273, 2019, doi: 10.1016/j.bsecv.2019.06.002.

[17]   M. Mia, M. Pervez, M. Hossain, M. R.-R. in physics, and undefined 2017, "Influence of Mg content on tailoring optical bandgap of Mg-doped ZnO thin film prepared by sol-gel method," *Elsevier*, Accessed: Aug. 08, 2019. [Online]. Available: https://www.sciencedirect.com/science/article/pii/S2211379717306022.

[18]   N. Abirami, A. M. S. Arulanantham, and K. S. J. Wilson, "Structural and magnetic properties of cobalt doped ZnO thin films deposited by cost effective nebulizer spray pyrolysis technique," *Mater. Res. Express*, vol. 7, no. 2, 2020, doi: 10.1088/2053-1591/ab6e27.

[19]   A. K. Vishwakarma and L. Yadava, "Fabrication and characterization of CdS doped ZnO nano thick films," *Vacuum*, vol. 155, pp. 214–218, 2018, doi: 10.1016/j.vacuum.2018.06.013.

[20]   A. Obeydavi, K. Dastafkan, M. Rahimi, M. Amin, and G. Dezfouli, "Insights into post-annealing and silver doping effects on the internal microstructure of ZnO nanoparticles through X-ray diffraction probe," *Solid State Sci.*, 2017, doi: 10.1016/j.solidstatesciences.2017.05.004.

[21]   G. S. Thool, A. K. Singh, R. S. Singh, A. Gupta, and M. A. B. H. Susan, "Facile synthesis of flat crystal ZnO thin films by solution growth method: A micro-structural investigation," *J. Saudi Chem. Soc.*, vol. 18, no. 5, pp. 712–721, 2014, doi: 10.1016/j.jscs.2014.02.005.

[22]   P. Kaur *et al.*, "Correlation between lattice deformations and optical properties of Ni doped ZnO at dilute concentration," *Mater. Today Proc.*, vol. 26, no. xxxx, pp. 3436–3441, 2019, doi: 10.1016/j.matpr.2019.12.001.

[23]   B. Du Ahn, H. S. Kang, J. H. Kim, G. H. Kim, H. W. Chang, and S. Y. Lee, "Synthesis and analysis of Ag-doped ZnO," *J. Appl. Phys.*, vol. 100, no. 9, 2006, doi: 10.1063/1.2364041.

[24]   Y. Wang, P. Xiao, H. Yang, S. Wang, R. Liu, and Y. Cao, "E ff ects of atom- and phase-scale compressive stress on fracture toughness in yttrium-doped lanthanum zirconate solid solutions," *Ceram. Int.*, vol. 44, no. 6, pp. 6590–6600, 2018, doi: 10.1016/j.ceramint.2018.01.062.

[25]   M. Caglar, Y. Caglar, S. Aksoy, and S. Ilican, "Temperature dependence of the optical band gap and electrical conductivity of sol-gel derived undoped and Li-doped ZnO films," *Appl. Surf. Sci.*, vol. 256, no. 16, pp. 4966–4971, 2010, doi: 10.1016/j.apsusc.2010.03.010.

[26]   M. Shirvani and L. Naji, "Effect of Seed Layer on the Morphology of Zinc Oxide Nanorods as an Electron Transport Layer in Polymer Solar Cells," vol. 16, no. 3, pp. 201–208, 2020.

[27]   D. Anbuselvan and S. Muthukumaran, "Defect related microstructure, optical and photoluminescence behaviour of Ni, Cu co-doped ZnO nanoparticles by co-precipitation method," *Opt. Mater. (Amst).*, vol. 42, pp. 124–131, 2015, doi: 10.1016/j.optmat.2014.12.030.

[28]   A. Kaushal, D. Pathak, R. K. Bedi, and D. Kaur, "Structural, electrical and optical properties of transparent Zn1 - xMgxO nanocomposite thin films," *Thin Solid Films*, vol. 518, no. 5, pp. 1394–1398, 2009, doi: 10.1016/j.tsf.2009.09.020.

[29]   G. El Hallani *et al.*, "Comparative study for highly Al and Mg doped ZnO thin films elaborated by sol gel method for photovoltaic application," *J. Appl. Phys.*, vol. 121, no. 13, 2017, doi: 10.1063/1.4979724.

[30]   M. Shirazi, R. Sabet Dariani, and M. R. Toroghinejad, "Influence of doping behavior of Al on nanostructure, morphology and optoelectronic properties of Al Doped ZnO thin film grown on FTO substrate," *J. Mater. Sci. Mater. Electron.*, vol. 27, no. 10, pp. 10226–10236, 2016, doi: 10.1007/s10854-016-5101-5.

[31]   M. Benhaliliba, C. E. Benouis, M. S. Aida, F. Yakuphanoglu, and A. S. Juarez, "Indium and aluminium-doped ZnO thin films deposited onto FTO substrates : nanostructure , optical , photoluminescence and electrical properties," pp. 335–342, 2010, doi: 10.1007/s10971-

010-2258-x.

[32]   X. Guo, Q. Zhang, X. Ding, and Q. Shen, "Synthesis and application of several sol – gel-derived materials via sol – gel process combining with other technologies : a review," *J. Sol-Gel Sci. Technol.*, vol. 79, no. 2, pp. 328–358, 2016, doi: 10.1007/s10971-015-3935-6.

[33]   J. Wang *et al.*, "Oxygen vacancy induced band-gap narrowing and enhanced visible light photocatalytic activity of ZnO," *ACS Appl. Mater. Interfaces*, vol. 4, no. 8, pp. 4024–4030, 2012, doi: 10.1021/am300835p.

[34]   H. Liu, F. Zeng, Y. Lin, G. Wang, and F. Pan, "Correlation of oxygen vacancy variations to band gap changes in epitaxial ZnO thin films," *Appl. Phys. Lett.*, vol. 102, no. 18, 2013, doi: 10.1063/1.4804613.

[35]   J. Herrero and C. Guille, "Influence of oxygen in the deposition and annealing atmosphere on the characteristics of ITO thin films prepared by sputtering at room temperature," vol. 80, pp. 615–620, 2006, doi: 10.1016/j.vacuum.2005.10.006.

[36]   J. Wang, L. Meng, Y. Qi, M. Li, G. Shi, and M. Liu, "The Al-doping contents dependence of the crystal growth and energy band structure in Al:ZnO thin films," *J. Cryst. Growth*, vol. 311, no. 8, pp. 2305–2308, 2009, doi: 10.1016/j.jcrysgro.2009.02.039.

[37]   M. Arshad, M. M. Ansari, and A. Ahmed, "Band gap engineering and enhanced photoluminescence of Mg doped ZnO nanoparticles synthesized by wet chemical route," *J. Lumin.*, vol. 161, pp. 275–280, 2015, Accessed: Aug. 08, 2019. [Online]. Available: https://www.sciencedirect.com/science/article/pii/S0022231314007212.